Redox Biology 43 (2021) 101984

Contents lists available at ScienceDirect

Redox Biology

journal homepage: www.elsevier.com/locate/redox

Iron overload in the motor cortex induces neuronal ferroptosis following spinal cord injury

Zhou Feng, Lingxia Min, Hui Chen, Weiwei Deng, Mingliang Tan, Hongliang Liu **, Jingming Hou *

Department of Rehabilitation, Southwest Hospital, Third Military Medical University (Army Medical University), Chongqing, China

ARTICLE INFO

Keywords:
Iron overload
Lipid peroxidation
Motor cortex
Ferroptosis
Spinal cord injury

ABSTRACT

Motor neuron death is supposed to result in primary motor cortex atrophy after spinal cord injury (SCI), which is relevant to poorer motor recovery for patients with SCI. However, the exact mechanisms of motor neuron death remain elusive. Here, we demonstrated that iron deposition in the motor cortex was significantly increased in both SCI patients and rats, which triggered the accumulation of lipid reactive oxygen species (ROS) and resulted in motor neuronal ferroptosis ultimately. While iron chelator, ROS inhibitor and ferroptosis inhibitor reduced iron overload-induced motor neuron death and promoted motor functional recovery. Further, we found that activated microglia in the motor cortex following SCI secreted abundant nitric oxide (NO), which regulated cellular iron homeostasis-related proteins to induce iron overload in motor neurons. Thus, we conclude that microglial activation induced iron overload in the motor cortex after SCI triggered motor neuronal ferroptosis and impeded motor functional recovery. These findings might provide novel therapeutic strategies for SCI.

1. Introduction

Spinal cord injury (SCI) is a highly disabling neurological disorder that often leads to permanent motor and sensory function deficits. It not only has a devastating impact on the life of patients, but impose a great burden on families and society [1]. Despite progress in both basic and clinical research of SCI in recent years, there is still a lack of effective treatments for the recovery of motor function after SCI.

Most previous studies have focused on the lesion site of SCI, but all strategies are far from satisfactory when translating to clinic [2]. Interestingly, our recent studies demonstrated that SCI causes significant structural atrophy and functional changes of the motor cortex in the early stage of disease [3,4]. Additionally, we further found that the degree of motor cortex atrophy after SCI was negatively correlated with the recovery level of motor function [5]. Hence, therapeutic strategies targeting structural and functional reorganization of the brain might be promising for SCI [6].

It was demonstrated that SCI can cause neuronal death in the motor cortex, which may be associated with atrophic changes of motor cortex following SCI [7,8]. The death of neurons in the motor cortex would presumably involve related axons (corticospinal tract), which may be an obstacle to achieve effective recovery from local treatment following SCI [9]. Although preventing the death of motor cortex neurons after SCI may be a potential strategy to promote the motor function recovery, the exact mechanism of neuronal death remains largely elusive.

In 2012, Dixon et al. firstly reported a new form of regulated cell death in cancer cells, which is distinct from apoptosis, necrosis and autophagy, and termed it ferroptosis [10]. This nonapoptotic cell death is characterized by iron-mediated, which triggers the accumulation of lipid reactive oxygen species that resulting in cell death ultimately [10]. Subsequent studies showed that ferroptosis has significant implications in various neurologic disorders [11–15]. Interestingly, our previous research has demonstrated that microglia activation and iron accumulation was induced by SCI in the brain [16,17]. Accordingly, these findings suggest that ferroptosis may be involved in the brain damage following SCI.

Here, we investigated whether SCI-induced intracranial iron overload triggers neuronal ferroptosis in the motor cortex, thus impairing the

* Corresponding author. Department of Rehabilitation, Southwest Hospital, Third Military Medical University (Army Medical University), No.30, Gaotanyan Street, Chongqing, 400038, PR China.

** Corresponding author. Department of Rehabilitation, Southwest Hospital, Third Military Medical University (Army Medical University), No.30, Gaotanyan Street, Chongqing, 400038, PR China.

E-mail addresses: liuhongliangkf@163.com (H. Liu), jingminghou@hotmail.com (J. Hou).

https://doi.org/10.1016/j.redox.2021.101984
Received 14 December 2020; Received in revised form 4 April 2021; Accepted 16 April 2021
Available online 22 April 2021

motor functional recovery, in an in vivo rat model of SCI and in vitro rat primary neurons. Moreover, we further explored the possible mechanism of iron overload caused by SCI.

2. Materials and methods

2.1. Patient magnetic resonance imaging (MRI)

The clinical study was approved by the medical ethics committee of Army Medical University (Chongqing, China), and all participants have given written informed consent. Susceptibility weighted imaging (SWI) was obtained from seventeen patients with SCI from the Department of Rehabilitation at the Southwest Hospital and sixteen healthy controls. The two groups were well-matched for age, gender, and years of education. Clinical and demographic data from all participants are shown in Supplementary Table 1. And detailed clinical characteristics of all SCI cases are listed in Supplementary Table 2. MRI was performed on a 3.0 T MR scanner (TIM Trio, Siemens Healthcare, Erlangen, Germany) with a twelve-channel phase-array head coil. SWI were obtained using a high-resolution three-dimensional spoiled gradient-echo sequence with the following parameters: TR/TE = 56/42; flip angle = 20°; section thickness = 2 mm; field of view = 23 × 17 cm; and matrix size = 348 × 320. The method for the analysis of iron deposition is detailed in previously published article [18]. Specifically, all images were analyzed by two independent radiologists using SPIN software. The selection of region of interest (ROI) was performed manually on the slice that showed the largest area of motor cortex. The average Siemens Phase Unit (SPU) of ROI were obtained and converted into radians by the following equation: (SPU-2048) x π/2048.

2.2. Animal preparation and groups

One hundred and ninety-five female Sprague–Dawley (SD) rats (Army Medical University) weighing 250–300 g were used in the present experimentation. All rats were maintained under a 12 h light/dark cycle pathogen-free condition with free access to food and water. Animal use protocols were approved by the Animal Care and Use Committee of the Army Medical University. The experiments in vivo were performed in 3 parts. In the first part, rats received SCI induction and were euthanized at days 1, 3, 7, 14 and 28 (n = 6 per time point) for iron content detection. In the second part, rats were randomly divided into Sham group, Vehicle group, deferoxamine (DFO) group, N-acetylcysteine (NAC) group and ferrostatin-1(Fer-1) group. DFO (5 mg/kg, diluted in saline, Sigma), NAC (40 μg/kg, diluted in saline, Sigma) and Fer-1 (40 μg/kg, diluted with 0.01% DMSO in saline, Sigma) were administered through intraventricular injection weekly and vehicle group received corresponding dose of 0.01% DMSO in saline. In the third part, rats were randomly divided into Sham group, SCI group, Vehicle group, minocycline (Mino) group and N(G)-nitro-L-arginine methyl ester (L-NAME) group. Minocycline (45 mg/kg, diluted in saline, Sigma) and L-NAME (50 mg/kg, diluted in saline, Sigma) were administered intraperitoneally weekly and vehicle group received corresponding dose of saline.

2.3. SCI model

The SCI model was induced via a clip-compression injury method as described previously [19]. Briefly, animals were anesthetized by intraperitoneal injection of pentobarbital (40 mg/kg). Using aseptic techniques, the vertebral column of the rats was exposed through a dorsal midline incision. After a T9 laminectomy, the spinal cord was compressed by a clip (50-g closing force) for 60 s to induce SCI. The sham control rats underwent the same procedure but no compression. Treatment rats received intraventricular injections sequentially, others were allowed to recover after surgical incision closure. All rats underwent manual bladder expression twice daily until the recovery of bladder control.

2.4. Intraventricular injection

Intraventricular injections were performed according to our previous method [20]. After anesthetized as previously mentioned, rats were transferred to a stereotactic frame. A 29-gauge needle was inserted into the right lateral ventricle (coordinates: 0.6 mm posterior, 4.5 mm ventral, and 1.6 mm lateral to the bregma) through a cranial hole drilled previously. The burr hole was plugged with bone wax followed by closing of skin incision.

2.5. Primary cultures of cortical neurons and drug treatments

Primary cortical neurons were generated from embryos of SD rats at embryonic day 20–21. Cerebral cortices were rapidly dissected and minced into small pieces. Then tissues were incubated in 0.25% trypsin ((Invitrogen) with 0.5 mg/ml DNase I (Roche) at 37 °C for 15 min. Next, the tissues were triturated with pipettes in Dulbecco's modified Eagle's medium (DMEM, Invitrogen) containing 10% fetal bovine serum. After trituration, tissue suspension was filtered through a strainer and centrifuged at 500 rpm for 5 min. Finally, the precipitated cortical neurons were cultured in neurobasal medium (Invitrogen) with 2% B27 Supplement, L-glutamine (1 μM), penicillin (100 U/ml) and streptomycin (0.1 mg/ml). The primary cortical neurons were cultured to day 9 for treatment. In the first part, cultured cortical neurons were treated with different concentrations (10, 50, 100 and 150 μM) of ferric ammonium citrate (FAC, Sigma) for 24 h to choose appropriate dose to establish an in vitro iron overload model. Then cortical neurons were treated with selected concentration of FAC with or without gradient concentrations of DFO (50, 100, 150 and 200 μM), NAC (10, 100, 200 and 500 μM) and Fer-1 (5, 10, 15 and 20 μM). Or cortical neurons were treated with RSL3 (5 μM) [21], with or without FAC and Fer-1. In the second part, cultured cortical neurons were incubated in the absence or presence of 250 μM (Z)-1-[N-(2-aminoethyl)-N-(2-ammonioethyl) amino]diazen-1-ium-1,2-diolate (DETA NONOate, Cayman), a NO donor, for 24 h. The concentration of DETA NONOate was chosen based on the previous study [22].

2.6. Cell viability assay

Cell viability was measured using Cell Counting Kit-8 (CCK8, Beyotime) according to the manufacturer's instructions. The optical density (OD) was assessed at a wavelength of 450 nm.

2.7. Motor cortex iron content assay

The iron content of the primary motor cortex (M1) was determined by colorimetric ferrozine-based assay with some modifications [23]. Briefly, after perfused transcardially with ice-cold PBS, the motor cortex was cut and weighed. Then the tissue was homogenized and 1 ml HCL (8.5 M) was added. The mixed sample was hydrolyzed at 95 °C for 1 h. After cooling to room temperature, 2 mL trichloroacetic acid (20%) was added to precipitate protein. Then sample was centrifuged and supernatant (220 μl) was mixed with 60 μl iron detection reagent (6.5 mM ferrozine, 6.5 mM neocuproine, 2.5 mM ammonium acetate, and 1 M ascorbic acid in H_20). The absorbance was measured at 562 nm 30 min latter and iron concentration was calculated by comparing to a standard curve. Iron concentrations were expressed as μg/g brain tissue.

2.8. Immunofluorescence

After deeply anesthetized, rats were perfused transcardially with ice-cold PBS and brains were collected. After fixed, dehydrated and embedded, brains were cut into 20-μm-thick coronal slices using a cryostat. Similarly, cultured neurons were harvested and fixed. Then slices or cultured neurons were blocked in 10% goat serum for 1 h at room temperature and then incubated with primary antibody against

Iba-1 (Wako, Japan) or microtubule-associated protein 2 (Map2; Abcam) at 4 °C overnight. After washed with phosphate-buffered solution (PBS), samples were incubated with appropriate secondary antibody at 37 °C for 3 h and cell nuclei were stained with DAPI. Stained sections were examined and images were captured using a confocal microscope (LSM-780; Zeiss).

2.9. Nissl staining

The prepared coronal brain sections were washed with distilled water and incubated in Nissl staining solution (Beyotime) for 10 min at 37 °C. Then sections were washed twice with distilled water for a few seconds, and dehydrated in turn with 95% and 100% ethanol for 3 min. After cleared with xylene for 5 min and sealed, stained sections were examined under a light microscope.

2.10. Stereological analysis

The number of Nissl-positive neurons in the motor cortex was stereologically estimated.

20-μm-thick coronal sections were serially cut throughout a certain region of the M1 (from -1.00 to 1.00 relative to bregma). Every tenth section was processed for Nissl staining. The estimated number of Nissl-positive neurons in each selected section was divided by the area of the region of interest to calculate cellular density expressed in cells/mm^2.

2.11. Western blot analysis

Western blot (WB)analysis was performed as previously described [20]. Briefly, brains were removed immediately after anesthetization and decapitation were performed. Samples were collected from the object region of brains and lysed in RIPA buffer containing protease and phosphatase inhibitors (Sigma). Then protein extract was obtained after centrifugation. Equal amounts of protein (40 mg) were loaded onto each lane of SDS-PAGE gels. After gel electrophoresis, proteins were transferred onto nitrocellulose membranes (Millipore) and blocked in nonfat milk at room temperature for 2 h. Then membranes were incubated in primary antibodies at 4 °C for 24 h and incubated in appropriate secondary antibodies at room temperature for 1 h subsequently. The following antibodies were used: Iba-1(Wako), iron regulatory protein 1 (IRP1, ZenBioScience), divalent metal transporter 1 (DMT1, MyBioSource), transferrin receptor1 (TfR1, ZenBioScience), ferritin (MyBioSource), ferroportin1 (Fpn1, MyBioSource), β-actin (ZenBioScience) and β-tubulin (ZenBioScience). Protein bands were visualized using nickel-intensified DAB solution, and band densitometry analysises were performed using Image J software (National Institutes of Health). The housekeeping proteins β-actin or β-tubulin were used as a loading control.

2.12. ROS production assay

ROS production was determined by flow cytometry using the fluorescent probe 2′,7′-dichlorodihydrofluorescein diacetate (H2DCFDA, MedChemExpress). After deeply anesthetized, rats were perfused transcardially with ice-cold PBS and M1 was harvested to obtain single-cell suspensions. Cultured primary cortical neurons were harvested by trypsinization after corresponding treatments. Cells were incubated with H2DCFDA (25 μM) at 37 °C for 30 min. After washed with PBS, cells were resuspended and analyzed by a flow cytometer (FACSuite, BD Biosciences).

2.13. Lipid peroxidation assay

Lipid peroxidation in brain homogenates was quantified using the malondialdehyde (MDA) assay kit (Beyotime) according to the manufacturer's instructions. Lipid peroxidation in cultured primary cortical neurons was analyzed using Liperfluo (Dojindo) or C11-BODIPY (581/591) (Invitrogen). After corresponding treatments and harvested by trypsinization, cells were incubated with Liperfluo (5 μM) or C11-BODIPY (581/591) (1 μM) at 37 °C for 30 min. Then cells were washed, resuspended and analyzed by a flow cytometer (FACSuite, BD Biosciences).

2.14. Nitric oxide (NO) assay

NO levels in M1 after SCI was tested using a NO assay kit (Beyotime) according to the manufacturer's instructions. The results were normalized to the protein concentration of each sample and expressed as nmol/mg protein.

2.15. Locomotion tests

Locomotor function was assessed using the Basso, Beattie and Bresnahan (BBB) locomotor test on day 1, 7, 14, 21,28 days after the operation [24]. Rats were placed in an open field area to move freely for 5 min and were observed by two blinded evaluators to evaluate motor function. The average score was calculated and finally taken.

2.16. Electrophysiological assessment

Motor evoked potentials (MEPs) was performed to evaluate the functional integrity of spinal pathways as previous described [25]. Rats were anesthetized with 1% pentobarbital sodium (20 mg/kg) intraperitoneally. One monopolar needle electrode was inserted subcutaneously at the base of the nose to act as the anode. Another electrode was inserted subcutaneously at the midpoint of the line between two ears, with its tip touching the bone, to act as the cathode. The recording electrode was inserted into the gastrocnemius muscle and the ground electrode was inserted subcutaneously at the base of the tail. A single electrical pulse (10 mA, 0.1 ms, 1 Hz) was delivered to excite the brain and the amplitude of MEPs was recorded.

2.17. Transmission electron microscope

Rats were perfused with 2% paraformaldehyde and 2% glutaraldehyde in 0.1 M sodium cacodylate. Brain samples were collected from removed brains and cut into sections (70–90 nm). Cultured primary neurons were fixed 2% glutaraldehyde in 0.1 M sodium cacodylate and cell samples were collected. After post-fixed in 2% osmium tetroxide, both brain and cell samples were stained with 2% uranyl acetate, dehydrated in ethanol, and then embedded in eponate. Finally, samples were placed on copper slot grids followed by stained with 2% uranyl acetate and lead citrate. Images were captured using transmission electron microscope (7600; Hitachi, Japan).

2.18. Real-time quantitative polymerase chain reaction

Total RNA was extracted from either brain tissue or cell cultures using the PureLink RNA kit (Thermo Fisher Scientific). Then quantitative PCR was performed using SYBR Green master mix (Life Technologies) according to the manufacturer's instructions. The following sequences of the primers were used: *Ptgs2*, forward, 5′-GGCCTCCATTGACCAGA-3′, reverse, 5′-CAGGGAGAAGCGTTTGC-3'; *Gpx4*, forward, 5′-GGACCTGCCGTGCTATCT-3′, reverse, 5′-GGCCTCTGGACCTTCCTC-3'; *Fsp1* (*Aifm2*), forward, 5′-CATAGCATGAGACCAAGGG-3′, reverse, 5′-GAGGGAAGGAAAGAAGACG-3'; *β-Actin*, forward, 5′- CCCATCTATGAGGGTTACGC-3′, reverse, 5′-TTTAATGTCACGCACGATTTC-3'. Relative expression was normalized to β-Actin and calculated using $2^{-\Delta\Delta CT}$.

2.19. Statistical analysis

All statistical analysis was performed by GraphPad Prism 6.0. Two

group comparisons were made by Student's *t*-test. Multigroup comparisons were analyzed using one-way analysis of variance (ANOVA) followed by Bonferroni post hoc test. Data are expressed as mean ± standard deviation (SD) and $P < 0.05$ was defined as statistical significance.

3. Results

3.1. SCI induces iron overload in the motor cortex

Brain iron concentration of humans was evaluated by SWI, a sensitive sequence for iron detecting, as previous described [18]. Iron deposition in the motor cortex, the region of interest shown in Fig. 1A, of patients with SCI was increased significantly compared to healthy controls (Fig. 1B). Consistent with the clinical results, we further demonstrated iron content in the motor cortex of rats increased gradually following SCI (Fig. 1C). These findings suggest that SCI induces iron overload in the motor cortex.

3.2. Iron overload causes ROS accumulation, lipid peroxidation, shrunken mitochondria and dysregulation of ferroptosis-related genes

We further determined if SCI induced iron overload causes ferroptosis. As the hallmarks of ferroptosis, ROS accumulation and lipid peroxidation were assayed by fluorescent probe H2DCFDA and MDA assay kit, respectively. It was demonstrated that both ROS and lipid peroxidation increased significantly in the motor cortex 4w after SCI, which was suppressed by iron chelator DFO, ROS inhibitor NAC and ferroptosis inhibitor Fer-1 (Fig. 2A, B and C). We next detected mitochondria morphological characteristics using transmission electron microscope. Large number of shrunken mitochondria were observed in M1 of SCI group, which was ameliorated by DFO, NAC and Fer-1 (Fig. 2D). Ferroptosis-related genes were evaluated by qRT-PCR. The expression of *Ptgs2* was upregulated but partially reversed by DFO, NAC and Fer-1 after SCI (Fig. 2E). While the expression of *Gpx4* was downregulated and partially reversed by Fer-1 (Fig. 2E). The expression of *Fsp1 was not changed* significantly following SCI (Fig. 2E).

To further validate whether iron overload contributes to neuronal ferroptosis, primary cortical neurons were treated with FAC after purity identification (Supplementary Fig. 1). We first treated neurons with gradient concentrations of FAC (10, 50, 100 and 150 μM) and selected appropriate concentration (100 μM) to use in the subsequent experiments according to cell viabilities (Supplementary Fig. 2A). Then we chose the appropriate concentrations of DFO (100 μM), NAC (200 μM) and Fer-1 (10 μM) using concentration gradient experiments (Supplementary Fig. 2B, C and D). Consistent with the results of in vivo experiment, ROS and lipid peroxidation were observed to increase significantly, which were evaluated by fluorescent probes H2DCFDA and Liperfluo, respectively (Fig. 3A and B). And both accumulation of ROS and lipid peroxidation were alleviated when treated neurons with DFO, NAC or Fer-1 simultaneously (Fig. 3A and B). Similarly, FAC treatment resulted in obvious shrunken mitochondria, upregulation of *Ptgs2* expression and downregulation of *Gpx4* expression, which were ameliorated by DFO, NAC or Fer-1 treatment (Fig. 3C and D). While *Fsp1* expression was *not changed* significantly (Fig. 3D). Considering the well-established pivotal role of GPX4 in ferroptosis, we treated cortical neurons with GPX4 inhibitor (RSL3) to establish a link between SCI and ferroptosis more sufficiently. Like FAC treatment, RSL3 induced significant cell death (Supplementary Fig. 3A) and lipid peroxidation (Supplementary Fig. 3B) in neurons, which were evaluated by CCK8 and fluorescent probe C11-BODIPY (581/591) respectively. What's more, the expression of *Ptgs2* was also upregulated after RSL3 treatment, which was alleviated significantly by Fer-1 (Supplementary Fig. 3C). While Fer-1 alone did not influence the cell viability and expression levels of *Ptgs2* and *Gpx4* (Supplementary Fig. 3A, C and D). Hence, both in vivo and in vitro experimental results suggest that SCI induced iron overload causes neuronal ferroptosis.

3.3. Inhibition of iron overload induced ferroptosis ameliorates neuronal death, improves integrity of motor pathway and locomotor recovery after SCI

We investigated the number of neurons in the motor cortex using Nissl staining. Stereological analysis results indicated that the number of Nissl-positive neurons decreased following SCI. As expected, DFO, NAC and Fer-1treatment significantly increased the number of neurons (Fig. 4A and B). The functional integrity of motor pathway was evaluated by MEPs. The amplitude of MEPs markedly reduced after SCI, which rebounded following DFO, NAC and Fer-1treatment (Fig. 5A and B). Then BBB test was performed to evaluate locomotor function.

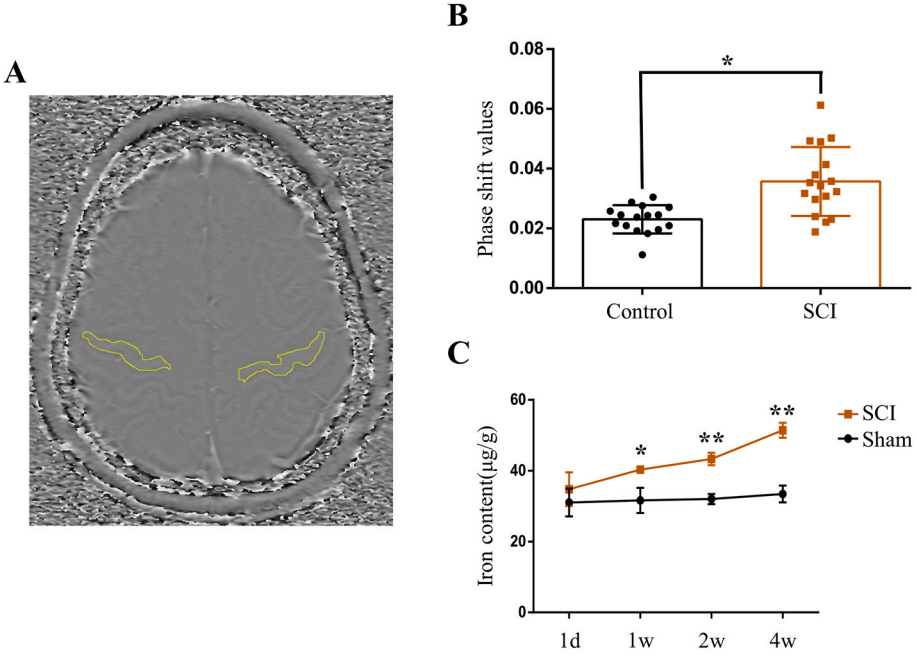

Fig. 1. SCI induces iron overload in the motor cortex. (A) Axial SWI phase image showing the regions of interest used in the quantitative analysis of iron content. (B) Phase shift values in the motor cortex of healthy controls (n = 16) and SCI patients (n = 17). Data are presented as means ± SD (*P < 0.05 versus control). (C) The iron content in the primary motor cortex (M1) of rats over time (1 day, 1, 2, 3 and 4 week) after SCI. Data are presented as means ± SD of n = 4 (*P < 0.05 and **P < 0.01versus sham).

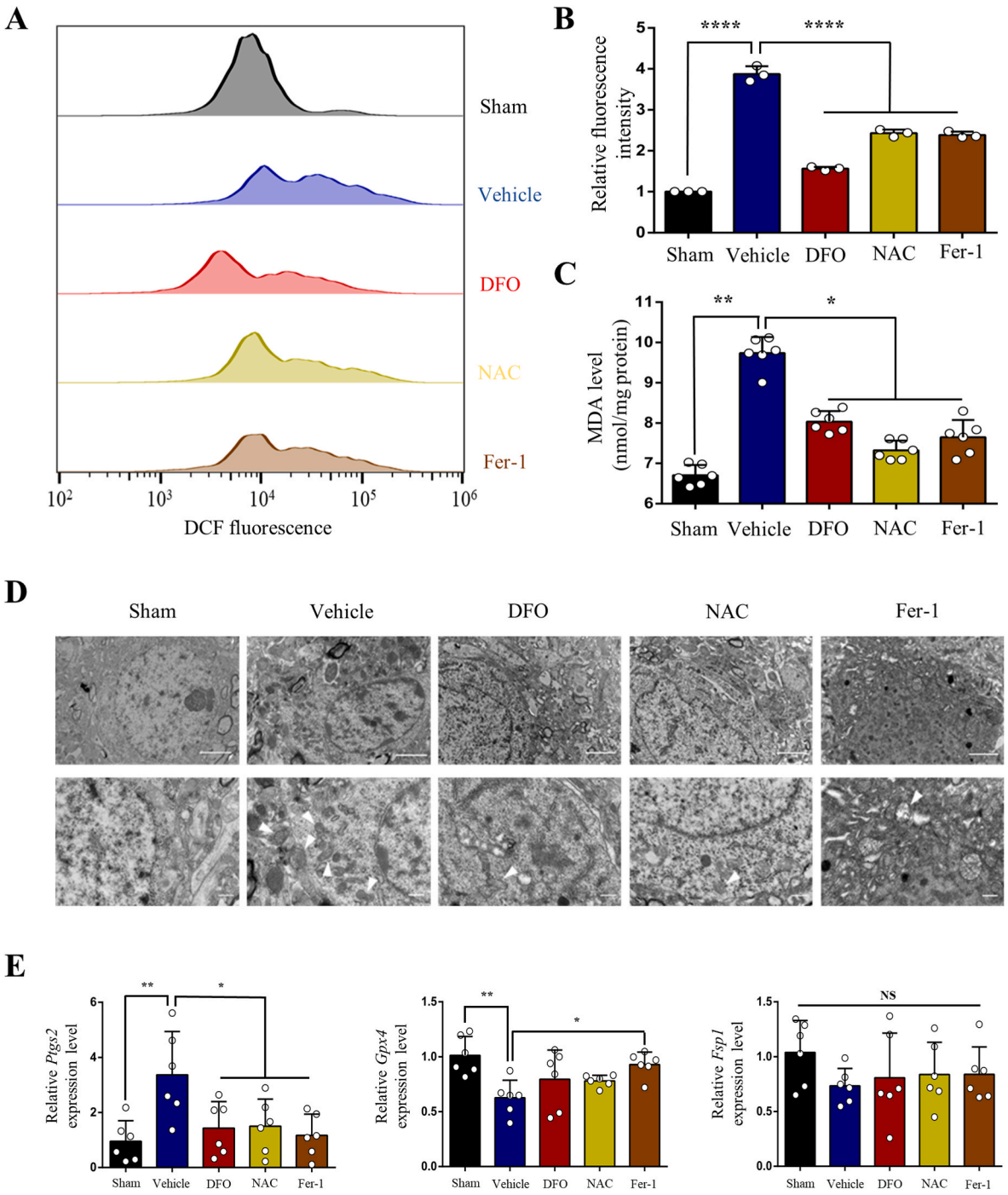

Fig. 2. Iron overload causes reactive oxygen species (ROS) accumulation, lipid peroxidation, shrunken mitochondria and dysregulation of ferroptosis-related genes after SCI. (A) and (B) ROS production in M1 4w after SCI was assessed by flow cytometry using H2DCFDA. Data are presented as means ± SD of n = 3 (****P < 0.0001 versus vehicle). (C) Lipid peroxidation in M1 after SCI was assessed by malondialdehyde (MDA) assay kit. Data are presented as means ± SD of n = 6 (*P < 0.05 and **P < 0.01 versus vehicle). (D) Transmission electron microscopy (TEM) and (E) mRNA expression of ferroptosis-related genes (*Ptgs2, Gpx4* and *Fsp1*) of M1 after SCI. Data are presented as means ± SD of n = 6 (NS = no significance; *P < 0.05 and **P < 0.01 versus vehicle). White arrowheads, shrunken mitochondria. Scale bars = 2 μm (above) or 500 nm (below).

Consistent with MEPs results, locomotor function severely impaired in SCI group, while DFO, NAC and Fer-1treatment significantly promoted functional recovery (Fig. 5C). Taken together, our results suggest that inhibiting ferroptosis by DFO, NAC and Fer-1 ameliorates neuronal death in the motor cortex, thus improves integrity of motor pathway and locomotor recovery after SCI.

3.4. SCI leads to iron metabolism dysfunction by elevating NO, which was released from activated microglia

Finally, we explored possible mechanism of how SCI induces iron overload in the motor cortex. Consistent with our previous study [17], we observed obvious microglia activation in the motor cortex after SCI, which was prevented by minocycline treatment (Fig. 6A, B and C). Unsurprisingly, activated microglia secreted abundant NO, and both

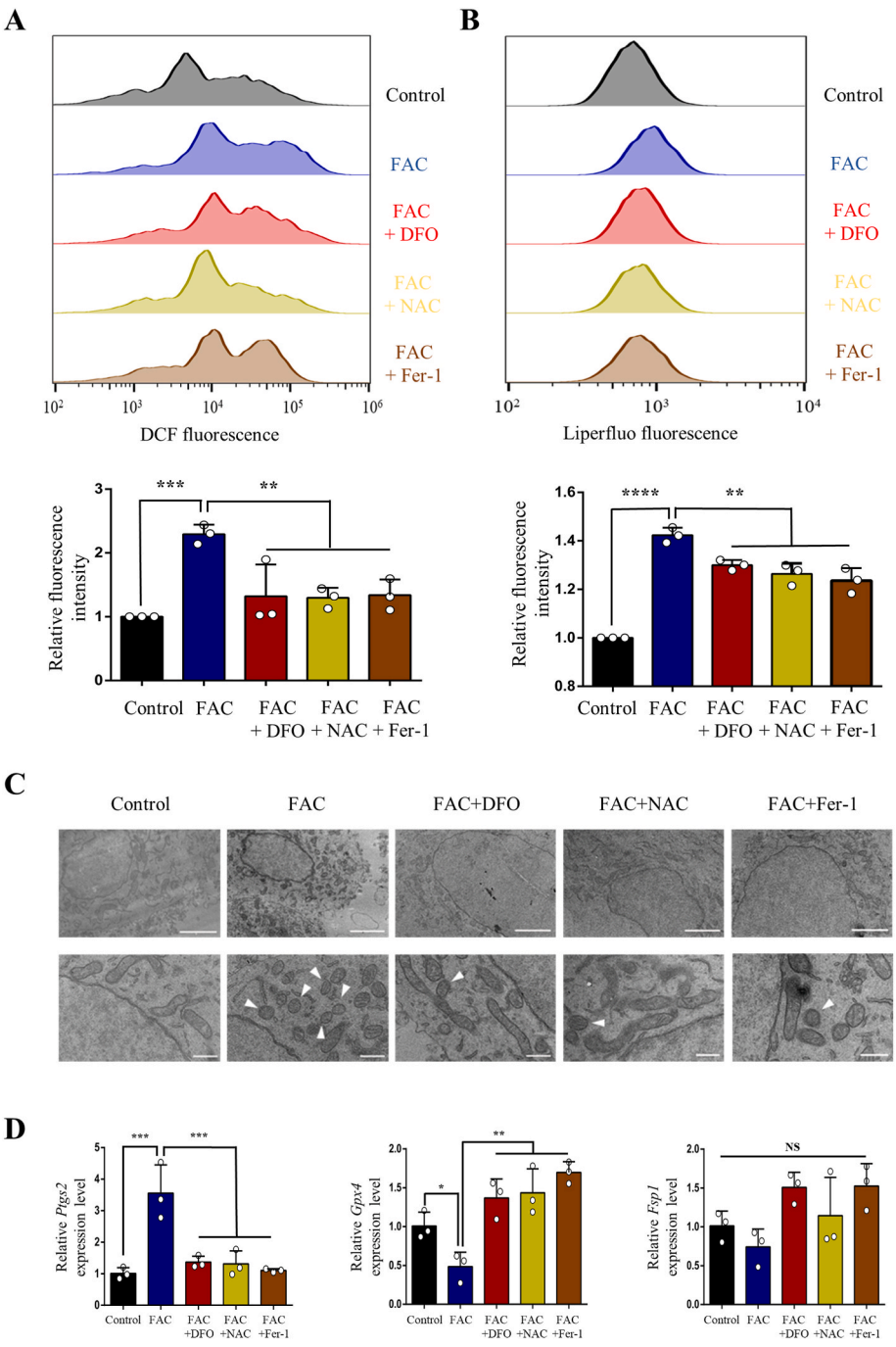

Fig. 3. Iron overload causes reactive oxygen species (ROS) accumulation, lipid peroxidation, shrunken mitochondria and dysregulation of ferroptosis-related genes in primary cortical neurons. (A) ROS production and (B) lipid peroxidation in cultured primary cortical neurons treated with or without ferric ammonium citrate (FAC, 100 μM), deferoxamine (DFO, 100 μM), N-acetylcysteine (NAC, 200 μM) and ferrostatin-1(Fer-1, 10 μM) was assessed by flow cytometry using H2DCFDA and Liperfluo, respectively. (C) TEM and (D) mRNA expression of ferroptosis-related genes (*Ptgs2, Gpx4* and *Fsp1*) of primary cortical neurons treated with or without FAC (100 μM), DFO (100 μM), NAC (200 μM) and Fer-1 (10 μM). Data are presented as means ± SD of n = 3 (NS = no significance; *P < 0.05, **P < 0.01, ***P < 0.001 and ****P < 0.0001 versus FAC). White arrowheads, shrunken mitochondria. Scale bars = 2 μm (above) or 500 nm (below).

minocycline and L-NAME treatment reduced NO level in the motor cortex (Fig. 6D). We next investigated iron metabolism-related proteins in the motor cortex by WB. We found increased expression of iron regulatory protein 1 (IRP1), divalent metal transporter 1 (DMT1) and transferrin receptor1 (TfR1) after SCI, that were all prevented by minocycline and L-NAME treatment (Fig. 7A, B, C and D). On the contrary, the expression of ferritin was decreased in SCI, but upregulated by minocycline and L-NAME (Fig. 7A and E). The expression of ferroportin1 (Fpn1) was increased after SCI, but was not significantly changed by neither minocycline nor L-NAME (Fig. 7A and F). And both minocycline and L-NAME significantly ameliorated SCI finally (Supplementary Fig. 4 A).

To further confirm whether NO contributes to iron dyshomeostasis via regulating iron metabolism-related proteins in vitro, we treated primary cortical neurons with NO donor. Consistent with results in vivo, superfluous NO up-regulated the expression of IRP1, DMT1 and TfR1, but down-regulated the expression of ferritin (Fig. 8A, B, C, D and E). The expression of Fpn1 was not significantly affected (Fig. 8A and F). What's more, superfluous NO finally triggered neuronal ferroptosis, that was alleviated by Fer-1(Supplementary Fig. 4 B, C and D). Therefore, our findings indicate that activated microglia secrete superfluous NO, which disturbs the expression of iron metabolism-related proteins and finally results in iron overload in the motor cortex after SCI.

4. Discussion

We have shown that intracranial iron overload induced by SCI caused neuronal ferroptosis in the motor cortex in in vivo and in vitro.

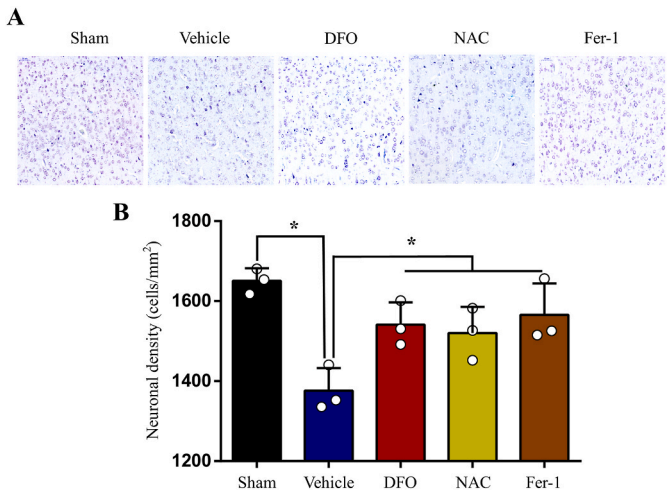

Fig. 4. Inhibition of ferroptosis ameliorates neuronal death after SCI. (A) Nissl staining in M1 following SCI. (B) Stereological analyses of Nissl-positive neurons in M1. Data are presented as means ± SD of n = 3 (*P < 0.05 versus vehicle).

Moreover, inhibition of ferroptosis diminished neuronal death and promoted motor functional recovery after SCI. Furthermore, we have demonstrated that iron metabolism dysfunction in the motor cortex following SCI was associated with increased IRP1, DMT1 and TfR1expression and decreased Ferritin expression, which was regulated by elevated levels of NO released from activated microglia. These findings indicate that inhibition of neuronal ferroptosis in the motor cortex might be a promising strategy to promote the motor function recovery after SCI.

Iron overload in the brain involves in the pathogenesis of various neurological disorders, including stroke, traumatic brain injury and neurodegenerative diseases [26–28]. Abnormal intracellular iron accumulation damages carbohydrates, lipids, proteins and DNA through generating free radicals and oxidative stress, which can induce cellular death subsequently [29]. Present study corroborates our previous finding, demonstrating that SCI causes iron overload in the motor cortex in both humans and animals. It highlights the unshrinkable responsibility of iron overload in the pathogenesis of SCI.

Excessive intracellular iron can cause mitochondrial damage and generation of reactive oxygen species (ROS) via Fenton reaction [30,31]. Accumulation of ROS will react with the polyunsaturated fatty acids (PUFAs) of lipid membranes to induce lethal lipid peroxidation, that triggers the non-apoptotic form of cell death named ferroptosis [10,31,32]. Moreover, iron was reported to promote production of lipid ROS via iron-catalyzed enzymatic manner and iron-containing lipoxygenases (LOXs) [33]. Consistent with previous findings, we detected iron-induced accumulation of lipid ROS both in the motor cortex of SCI rats and in primary neurons treated with FAC in our present study.

Ferroptosis is a newly discovered type of cell death that has attracted tremendous attention since discovered [34]. It is obviously distinct from other types of cell death biochemically, morphologically and genetically [10,35]. Correlating with its biological process described above, ferroptosis is characterized by iron-dependent accumulation of lethal lipid ROS biochemically [10]. Morphologically, we observed shrunken mitochondria with increased membrane density under TEM in both in vivo and in vitro, which was consistent with previous reports [10,36]. Ferroptosis was demonstrated to be regulated by a distinct set of genes, including *Ptgs2, Gpx4, Fsp1* and so on [10,37–39]. *Ptgs2*, a gene that encodes cyclooxygenase-2 (COX-2), was significantly upregulated during ferroptosis [37]. Moreover, expression of *Ptgs2* was reported to be upregulated in brain after stroke and traumatic brain injury (TBI) [11,40]. This is in agreement with our present study demonstrating that *Ptgs2* was upregulated in the motor cortex after SCI. These findings indicate that *Ptgs2* is closely related to ferroptosis [37,41]. Glutathione peroxidase 4 (GPX4) is a selenoprotein that considered to be a central regulator of ferroptosis [35,37,42]. By converting toxic lipid hydroperoxides to non-toxic lipid alcohols, GPX4 effectively prevents ferroptosis [43]. And Ishraq et al. showed that driving the expression of *Gpx4* via selenium supplementation protects neurons from ferroptosis and improves behavior in stroke [13]. Likewise, we found that *Gpx4* expression was decreased after SCI, and regulating *Gpx4* might be a promising therapeutic option for neurological disorders associated with ferroptosis, including SCI. Ferroptosis suppressor protein 1 (*Fsp1*), known as apoptosis-inducing factor mitochondrial 2 (*Aifm2*) previously, was identified as a ferroptosis suppressor that acts in parallel to *Gpx4* in two back-to-back studies by Bersuker et al. [39] and Doll et al. [38] in 2019. Functioning as an NADH-dependent oxidoreductase, *Fsp1* reduces coenzyme Q10 to suppress lipid peroxidation, thus preventing ferroptosis [38,39]. Although the *Fsp1* expression was not significantly changed

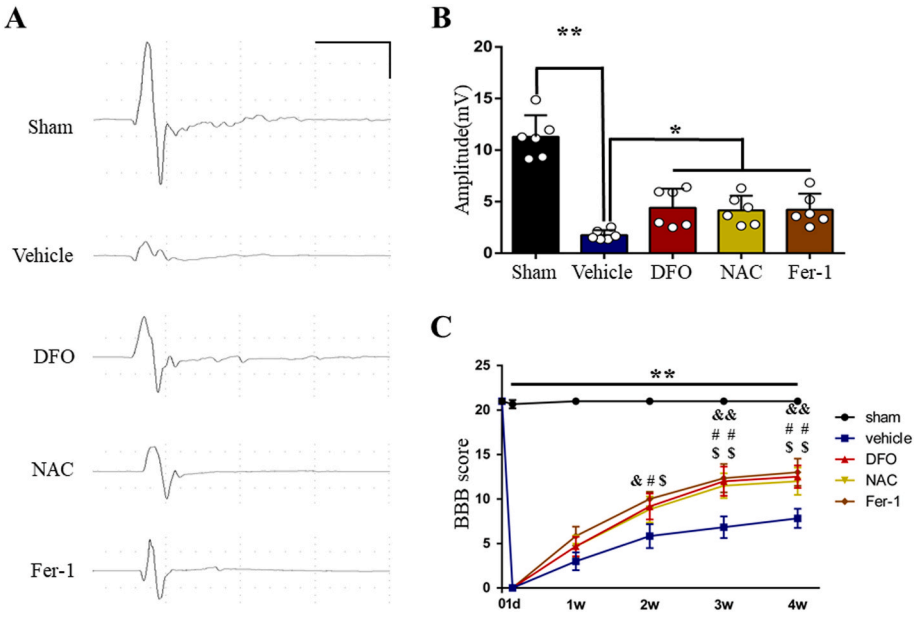

Fig. 5. Inhibition of ferroptosis improves integrity of motor pathway and locomotor recovery after SCI. (A) Representative recording of Motor evoked potentials (MEPs) from each group. Scale: 5 mV/10 ms. (B) The amplitudes of MEPs of each group. Data are presented as means ± SD of n = 6 (*P < 0.05 and **P < 0.01 versus vehicle). (C) The BBB scores of each group at different time points. Data are presented as means ± SD of n = 6 (**P < 0.01 sham versus vehicle, &P < 0.05 and &&P < 0.01 DFO versus vehicle, #P < 0.05 and ##P < 0.01 NAC versus vehicle, $P < 0.05 and $ $P < 0.01 Fer-1 versus vehicle).

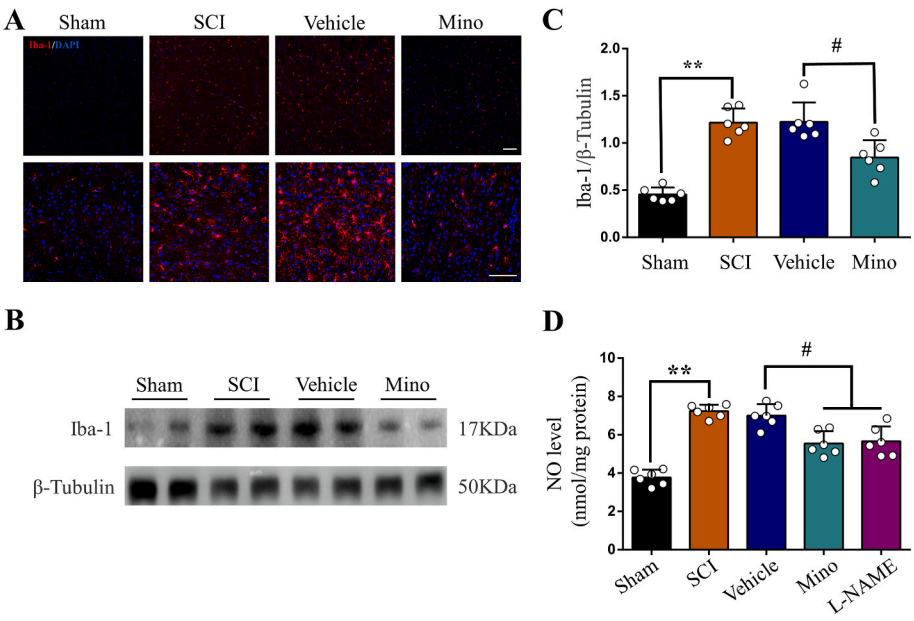

Fig. 6. SCI activates microglia to secrete NO in M1. (A) Representative images of Iba1(+) microglia (red) in M1 of each group. Nuclear was marked with DAPI (blue). (B) Representative Western blot bands and (C) quantitative analyses of Iba1 in M1 of each group. Data are presented as means ± SD of n = 6 (**P < 0.01 sham versus SCI, #P < 0.05 Mino versus vehicle). (D) NO levels in M1 of each group. Data are presented as means ± SD of n = 6 (**P < 0.01 sham versus SCI, #P < 0.05 Mino and L-NAME versus vehicle). . (For interpretation of the references to color in this figure legend, the reader is referred to the Web version of this article.)

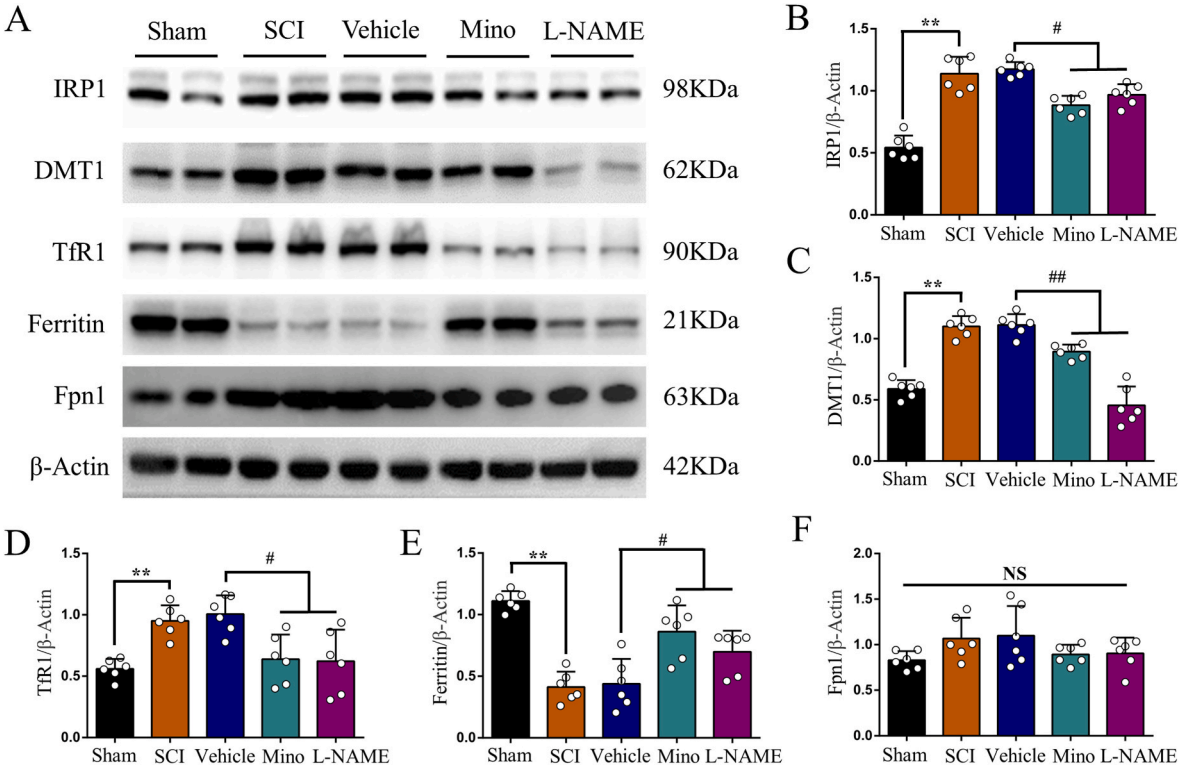

Fig. 7. SCI induced NO elevation disturbs the expression of iron metabolism-related proteins in M1. (A) Representative Western blot bands and quantitative analyses of (B) IRP1, (C) DMT1, (D) TfR1, (E) ferritin and (F) Fpn1 of each group. Data are presented as means ± SD of n = 6 (NS = no significance; **P < 0.01 sham versus SCI, #P < 0.05 and ##P < 0.01 Mino and L-NAME versus vehicle).

after SCI, its up-regulation might be beneficial. And considering the extensive involvement of iron-dependent ferroptosis in neurological disorders, identification of FSP1 might offer novel neuroprotective treatments [44].

It was reported that spinal cord injury causes apoptosis of neurons in the motor cortex [7]. In the present study, we found that iron overload induced neuronal ferroptosis in the in the motor cortex also leads to significant decrease in the number of surviving neurons. More interestingly, it is extremely likely to be the reason of motor cortex atrophy after SCI [3,5]. When neuronal ferroptosis was prevented, motor recovery was significantly promoted. This is in agreement with our previous study, demonstrating that motor recovery after SCI is related to brain cortical thickness [5].

Intracellular iron homeostasis in the brain is elaborately regulated by a full complement of iron proteins, including iron regulatory proteins (IRPs), divalent metal transporter 1 (DMT1), transferrin receptors (TfRs), ferritin and ferroportin1 (Fpn1) [45]. Neurons uptake iron through TfRs and DMT1, and then store it in ferritin or export it through

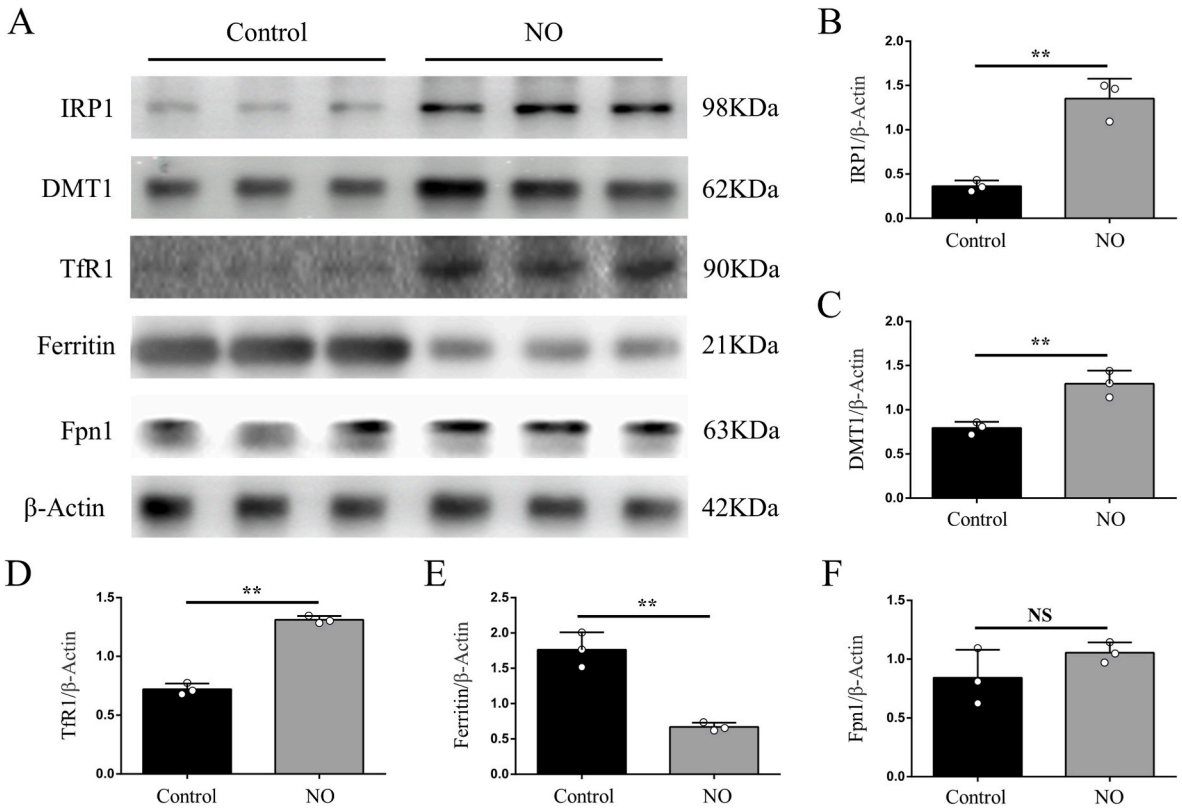

Fig. 8. Superfluous NO disturbs the expression of iron metabolism-related proteins in primary cortical neurons. (A) Representative Western blot bands and quantitative analyses of (B) IRP1, (C) DMT1, (D) TfR1, (E) ferritin and (F) Fpn1 of each group. Data are presented as means ± SD of n = 6 (NS = no significance; **P < 0.01).

Fpn1 [29,45]. The IRPs-iron responsive elements (IREs) system modulates intracellular iron metabolism via regulating translation of iron proteins above [46]. NO is a recognized free radical that can disturb cellular iron homeostasis by modulating IRP1-IRE signaling pathway [47]. Elevated NO, that was released from activated microglia, was supposed to be a causative factor of iron overload in various neurological disorders [47–49]. Moreover, iron accumulation in turn promotes microglia activation to aggravate damage [17]. In the current study, microglia reactivation and proliferation in the motor cortex was evoked after SCI, which was accompanied by elevated levels of NO. As expected, the expression of IRP1, TfR1 and DMT1 was increased while ferritin was decreased. We further tested the regulatory activity of NO on iron proteins in primary neurons treated with NO donor and obtained consistent results. And both treatment with minocycline (a microglia activation inhibitor) and L-NAME (a NO synthase inhibitor) reversed dysregulation of iron metabolism-related proteins and prevented iron overload in brain following SCI. Finally, NO induced iron overload triggers neuronal ferroptosis, which was alleviated by Fer-1. In addition to induce ferroptosis demonstrated in present study, NO was reported to contributed to various forms of neuronal death, including necrosis, apoptosis and so on [50]. This may be why Fer-1 could not prevent NO induced neuronal death adequately.

Continuing to our previous studies which indicated SCI induced motor cortex atrophy limits the functional recovery, the present work explored the potential mechanism of motor cortex atrophy caused by SCI. Iron overload induced neuronal ferroptosis reduces the number of neurons in the motor cortex, which is finally manifested as structural atrophy. Notably, as the ferroptosis of neurons, the corresponding axons will die as well [51]. This might be the reason why current therapeutic approaches that target for the injured spinal cord are far from satisfactory. Thus, therapeutic strategies focus on both injured spinal cord and brain is speculated to be the future of spinal cord injury treatment.

In summary, the present study revealed iron overload in the motor cortex, which was induced by NO released from activated microglia via regulating iron metabolism-related proteins, triggers neuronal ferroptosis to inhibit motor functional recovery after SCI. Therefore, our findings demonstrate that preventing iron-dependent neuronal ferroptosis in the motor cortex may be a potential therapeutic treatment for promoting motor functional recovery after SCI. Further studies are needed to investigate whether it is also effective in other SCI models and humans, and to understand the exact molecular mechanism involved in iron-induced neuronal ferroptosis in SCI.

Declaration of competing interest

All authors indicate no conflicts of interest.

Funding support

This work was supported by National Natural Science Foundation of China (81671211, 81672251), China; Talent Project of Southwest Hospital (2017MPRC-08), China.

Appendix A. Supplementary data

Supplementary data to this article can be found online at https://doi.org/10.1016/j.redox.2021.101984.

References

[1] C.S. Ahuja, J.R. Wilson, S. Nori, M.R.N. Kotter, C. Druschel, A. Curt, et al., Traumatic spinal cord injury, Nat. Rev. Dis. Primers 3 (2017) 17018.
[2] C.S. Ahuja, A.R. Martin, M.G. Fehlings, Recent advances in managing a spinal cord injury secondary to trauma, F1000Research. 5 (2016) 1017.

[3] J.M. Hou, R.B. Yan, Z.M. Xiang, H. Zhang, J. Liu, Y.T. Wu, et al., Brain sensorimotor system atrophy during the early stage of spinal cord injury in humans, Neuroscience 266 (2014) 208–215.
[4] J.M. Hou, T.S. Sun, Z.M. Xiang, J.Z. Zhang, Z.C. Zhang, M. Zhao, et al., Alterations of resting-state regional and network-level neural function after acute spinal cord injury, Neuroscience 277 (2014) 446–454.
[5] J. Hou, Z. Xiang, R. Yan, M. Zhao, Y. Wu, J. Zhong, et al., Motor recovery at 6 months after admission is related to structural and functional reorganization of the spine and brain in patients with spinal cord injury, Hum. Brain Mapp. 37 (6) (2016) 2195–2209.
[6] M. Sawada, K. Kato, T. Kunieda, N. Mikuni, S. Miyamoto, H. Onoe, et al., Function of the nucleus accumbens in motor control during recovery after spinal cord injury, Science (New York, NY) 350 (6256) (2015) 98–101.
[7] B.H. Lee, K.H. Lee, U.J. Kim, D.H. Yoon, J.H. Sohn, S.S. Choi, et al., Injury in the spinal cord may produce cell death in the brain, Brain Res. 1020 (1–2) (2004) 37–44.
[8] J. Wu, Z. Zhao, B. Sabirzhanov, B.A. Stoica, A. Kumar, T. Luo, et al., Spinal cord injury causes brain inflammation associated with cognitive and affective changes: role of cell cycle pathways, J. Neurosci. 34 (33) (2014) 10989–11006.
[9] F.M. Mar, A. Bonni, M.M. Sousa, Cell intrinsic control of axon regeneration, EMBO Rep. 15 (3) (2014) 254–263.
[10] S.J. Dixon, K.M. Lemberg, M.R. Lamprecht, R. Skouta, E.M. Zaitsev, C.E. Gleason, et al., Ferroptosis: an iron-dependent form of nonapoptotic cell death, Cell 149 (5) (2012) 1060–1072.
[11] B.S. Xie, Y.Q. Wang, Y. Lin, Q. Mao, J.F. Feng, G.Y. Gao, et al., Inhibition of ferroptosis attenuates tissue damage and improves long-term outcomes after traumatic brain injury in mice, CNS Neurosci. Ther. 25 (4) (2019) 465–475.
[12] A. Ashraf, J. Jeandriens, H.G. Parkes, P.W. So, Iron dyshomeostasis, lipid peroxidation and perturbed expression of cystine/glutamate antiporter in Alzheimer's disease: evidence of ferroptosis, Redox Biol. 32 (2020) 101494.
[13] I. Alim, J.T. Caulfield, Y. Chen, V. Swarup, D.H. Geschwind, E. Ivanova, et al., Selenium drives a transcriptional adaptive program to block ferroptosis and treat stroke, Cell 177 (5) (2019) 1262–1279 e25.
[14] N. Yan, J.J. Zhang, The emerging roles of ferroptosis in vascular cognitive impairment, Front. Neurosci. 13 (2019) 811.
[15] B. Do Van, F. Gouel, A. Jonneaux, K. Timmerman, P. Gele, M. Petrault, et al., Ferroptosis, a newly characterized form of cell death in Parkinson's disease that is regulated by PKC, Neurobiol. Dis. 94 (2016) 169–178.
[16] F.X. Meng, J.M. Hou, T.S. Sun, Effect of oxidative stress induced by intracranial iron overload on central pain after spinal cord injury, J. Orthop. Surg. Res. 12 (1) (2017) 24.
[17] F.X. Meng, J.M. Hou, T.S. Sun, In vivo evaluation of microglia activation by intracranial iron overload in central pain after spinal cord injury, J. Orthop. Surg. Res. 12 (1) (2017) 75.
[18] C. Liu, C. Li, J. Yang, L. Gui, L. Zhao, A.C. Evans, et al., Characterizing brain iron deposition in subcortical ischemic vascular dementia using susceptibility-weighted imaging: an in vivo MR study, Behav. Brain Res. 288 (2015) 33–38.
[19] L.C. Weaver, P. Verghese, J.C. Bruce, M.G. Fehlings, N.R. Krenz, D.R. Marsh, Autonomic dysreflexia and primary afferent sprouting after clip-compression injury of the rat spinal cord, J. Neurotrauma 18 (10) (2001) 1107–1119.
[20] Z. Feng, Q. Tan, J. Tang, L. Li, Y. Tao, Y. Chen, et al., Intraventricular administration of urokinase as a novel therapeutic approach for communicating hydrocephalus, Transl. Res. : J. Lab. Clin. Med. 180 (2017) 77–90.e2.
[21] C.W. Brown, J.J. Amante, P. Chhoy, A.L. Elaimy, H. Liu, L.J. Zhu, et al., Prominin2 drives ferroptosis resistance by stimulating iron export, Dev. Cell 51 (5) (2019) 575–586 e4.
[22] G.A. Benavides, Q. Liang, M. Dodson, V. Darley-Usmar, J. Zhang, Inhibition of autophagy and glycolysis by nitric oxide during hypoxia–reoxygenation impairs cellular bioenergetics and promotes cell death in primary neurons, Free Radic. Biol. Med. 65 (2013) 1215–1228.
[23] J. Riemer, H.H. Hoepken, H. Czerwinska, S.R. Robinson, R. Dringen, Colorimetric ferrozine-based assay for the quantitation of iron in cultured cells, Anal. Biochem. 331 (2) (2004) 370–375.
[24] D.M. Basso, M.S. Beattie, J.C. Bresnahan, A sensitive and reliable locomotor rating scale for open field testing in rats, J. Neurotrauma 12 (1) (1995) 1–21.
[25] B. Chen, Q. Tan, W. Zhao, Q. Yang, H. Zhang, F. Gao, et al., Diffusion tensor imaging and electrophysiology as robust assays to evaluate the severity of acute spinal cord injury in rats, BMC Neurol. 20 (1) (2020) 236.
[26] S. Cao, Y. Hua, R.F. Keep, N. Chaudhary, G. Xi, Minocycline effects on intracerebral hemorrhage-induced iron overload in aged rats, Stroke 49 (4) (2018) 995–1002.
[27] M. Daglas, P.A. Adlard, The involvement of iron in traumatic brain injury and neurodegenerative disease, Front. Neurosci. 12 (2018) 981.
[28] A. Drecourt, J. Babdor, M. Dussiot, F. Petit, N. Goudin, M. Garfa-Traoré, et al., Impaired transferrin receptor palmitoylation and recycling in neurodegeneration with brain iron accumulation, Am. J. Hum. Genet. 102 (2) (2018) 266–277.
[29] R.J. Ward, F.A. Zucca, J.H. Duyn, R.R. Crichton, L. Zecca, The role of iron in brain ageing and neurodegenerative disorders, Lancet Neurol. 13 (10) (2014) 1045–1060.
[30] N. Sumneang, N. Siri-Angkul, S. Kumfu, S.C. Chattipakorn, N. Chattipakorn, The effects of iron overload on mitochondrial function, mitochondrial dynamics, and ferroptosis in cardiomyocytes, Arch. Biochem. Biophys. 680 (2020) 108241.
[31] J.Y. Cao, S.J. Dixon, Mechanisms of ferroptosis, Cell. Mol. Life Sci. 73 (11–12) (2016) 2195–2209.
[32] G. Miotto, M. Rossetto, M.L. Di Paolo, L. Orian, R. Venerando, A. Roveri, et al., Insight into the mechanism of ferroptosis inhibition by ferrostatin-1, Redox Biol. 28 (2020), 101328.
[33] P. Lei, T. Bai, Y. Sun, Mechanisms of ferroptosis and relations with regulated cell death: a review, Front. Physiol. 10 (2019) 139.
[34] J. Li, F. Cao, H.L. Yin, Z.J. Huang, Z.T. Lin, N. Mao, et al., Ferroptosis: past, present and future, Cell Death Dis. 11 (2) (2020) 88.
[35] B.R. Stockwell, J.P. Friedmann Angeli, H. Bayir, A.I. Bush, M. Conrad, S.J. Dixon, et al., Ferroptosis: a regulated cell death nexus linking metabolism, redox biology, and disease, Cell 171 (2) (2017) 273–285.
[36] N. Yagoda, M. von Rechenberg, E. Zaganjor, A.J. Bauer, W.S. Yang, D.J. Fridman, et al., RAS-RAF-MEK-dependent oxidative cell death involving voltage-dependent anion channels, Nature 447 (7146) (2007) 864–868.
[37] S. Yang Wan, R. SriRamaratnam, E. Welsch Matthew, K. Shimada, R. Skouta, S. Viswanathan Vasanthi, et al., Regulation of ferroptotic cancer cell death by GPX4, Cell 156 (1–2) (2014) 317–331.
[38] S. Doll, F.P. Freitas, R. Shah, M. Aldrovandi, M.C. da Silva, I. Ingold, et al., FSP1 is a glutathione-independent ferroptosis suppressor, Nature 575 (7784) (2019) 693–698.
[39] K. Bersuker, J.M. Hendricks, Z. Li, L. Magtanong, B. Ford, P.H. Tang, et al., The CoQ oxidoreductase FSP1 acts parallel to GPX4 to inhibit ferroptosis, Nature 575 (7784) (2019) 688–692.
[40] Q. Li, X. Han, X. Lan, Y. Gao, J. Wan, F. Durham, et al., Inhibition of neuronal ferroptosis protects hemorrhagic brain, JCI Insight 2 (7) (2017) e90777-e.
[41] Y. Xie, W. Hou, X. Song, Y. Yu, J. Huang, X. Sun, et al., Ferroptosis: process and function, Cell Death Differ. 23 (3) (2016) 369–379.
[42] I. Ingold, C. Berndt, S. Schmitt, S. Doll, G. Poschmann, K. Buday, et al., Selenium utilization by GPX4 is required to prevent hydroperoxide-induced ferroptosis, Cell 172 (3) (2018) 409–422 e21.
[43] M. Maiorino, M. Conrad, F. Ursini, GPx4, lipid peroxidation, and cell death: discoveries, rediscoveries, and open issues, Antioxidants Redox Signal. 29 (1) (2018) 61–74.
[44] L. Chen, J. Xie, Ferroptosis-suppressor-protein 1: a potential neuroprotective target for combating ferroptosis, Mov. Disord. : Off. J. Movement Disorder Soc. 35 (3) (2020) 400.
[45] T.A. Rouault, Iron metabolism in the CNS: implications for neurodegenerative diseases, Nat. Rev. Neurosci. 14 (8) (2013) 551–564.
[46] Z.D. Zhou, E.K. Tan, Iron regulatory protein (IRP)-iron responsive element (IRE) signaling pathway in human neurodegenerative diseases, Mol. Neurodegener. 12 (1) (2017) 75.
[47] Q. Lu, V.A. Harris, R. Rafikov, X. Sun, S. Kumar, S.M. Black, Nitric oxide induces hypoxia ischemic injury in the neonatal brain via the disruption of neuronal iron metabolism, Redox Biol. 6 (2015) 112–121.
[48] K. Lepka, K. Volbracht, E. Bill, R. Schneider, N. Rios, T. Hildebrandt, et al., Iron-sulfur glutaredoxin 2 protects oligodendrocytes against damage induced by nitric oxide release from activated microglia, Glia 65 (9) (2017) 1521–1534.
[49] S. Ayton, P. Lei, Parkinson's disease iron deposition caused by nitric oxide-induced loss of β-amyloid precursor protein 35 (8) (2015) 3591–3597.
[50] G.C. Brown, Nitric oxide and neuronal death, Nitric Oxide 23 (3) (2010) 153–165.
[51] G.D. Carlson, C.D. Gorden, S. Nakazowa, E. Wada, K. Warden, J.C. LaManna, Perfusion-limited recovery of evoked potential function after spinal cord injury, Spine 25 (10) (2000) 1218–1226.